The International Journal of Advanced Manufacturing Technology (2019) 101:2837–2848
https://doi.org/10.1007/s00170-018-3015-5

ORIGINAL ARTICLE

Characterizing the effect of process variables on energy consumption in end milling

Lirong Zhou[1] · Fangyi Li[1] · Fu Zhao[2] · Jianfeng Li[1] · John W. Sutherland[2]

Received: 4 June 2018 / Accepted: 6 November 2018 / Published online: 12 December 2018

Abstract
Manufacturing processes, such as machining, transform raw materials into finished goods, and these processes consume significant energy. There is an increasing concern about the energy required for such processes and the environmental consequences attributable to the generation of the energy. Reducing the energy required to perform machining operations will not only reduce the environmental footprint, but also provide economic benefits. To that end, the effects of cutting conditions (e.g., feed and speed) and tool geometry (diameter and number of teeth) on the power required for an end milling operation are investigated experimentally. Experimental results are presented from a cutting mechanism perspective with the goal of understanding the role of the process variables. The specific cutting energy (SCE) is found decreasing when material removal rate increases, but there is substantial variation about the general trend. In essence, the cutting parameters and the tool geometry influenced the changes of average chip thickness and cutting speed, which cause the shear deformation energy changes and eventually collectively influence the SCE's change. Based on the experiments, suggestions on selecting process parameters are provided to improve milling energy efficiency.

Keywords Specific cutting energy · Average chip thickness · Energy efficiency of milling · Green manufacturing

1 Introduction

Global climate change and the depletion of fossil-fuel energy carriers are environmental impacts linked to the industrial consumption of energy. The IEA has declared that energy production is the largest man-made source of air pollutants, and much of the energy demand is associated with the industry sector [1]. Efforts such as increasing energy efficiency, increasing utilization of low-carbon technologies, and more stringent emission control regulations have led to the reduction of carbon dioxide (CO_2) and other airborne emissions in many industrial countries, and this trend is expected to continue [1].

Machine tools are widely used in manufacturing, and since they consume large amounts of electricity, they are responsible for large amounts of carbon dioxide emissions [2]. The European Union's Eco-design Directive 2009/125/E has taken machine tools as regulatory priority category, and the International Organization for Standardization drafted ISO 14955-1, which focuses on the energy consumption and environmental impact of machine tools. Reducing the energy consumption during the machining process is one approach to reduce the environmental impact of manufacturing [3], and research on this topic has gained wide attention.

Understanding how machining process parameters affect energy consumption is a key first step to improve the energy efficiency of machine tools and reduce energy waste. In recent decades, much research has been performed in this area. One

✉ Fangyi Li
lifangyi@sdu.edu.cn

Lirong Zhou
zhoulirong2012@qq.com

Fu Zhao
fzhao@purdue.edu

Jianfeng Li
ljf@sdu.edu.cn

John W. Sutherland
jwsuther@purdue.edu

[1] Key Laboratory of High Efficiency and Clean Mechanical Manufacture Ministry of Education, School of Mechanical Engineering, Shandong University, Jinan 250061, China

[2] Environmental and Ecological Engineering, Purdue University, West Lafayette, IN 47907, USA

of the most commonly adopted approaches is focused on specific cutting energy (SCE). SCE (also referred to as the cutting pressure) refers to the amount of energy needed by a cutting tool to remove a unit volume of a material. Alternatively, specific cutting energy can be expressed as the ratio of the cutting power to the material removal rate (MRR). SCE values may be thought of as describing the energy efficiency of the metal cutting process and also communicate the machinability of the material [4].

Previous work shows that SCE is a function of cutting parameters, tool geometry, tool finish, workpiece material properties, and cutting temperature [5]. From the view of chip formation mechanics, the SCE consists of the following components:

1) Shear deformation energy (primary shear zone and secondary shear zone deformation energy)
2) The friction energy between the chip and tool
3) Chip curl/bending energy
4) Chip kinetic energy
5) Energy to produce a new surface

As an approximation, the SCE can largely be expressed as a function of the first two components: the shear deformation energy and the friction energy [6]. Merchant [7], Shaw [8], Oxley [9], and other scholars have made outstanding contributions to the metal-cutting mechanics and cutting energy theory. Over the past 30 years, SCE models have been refined by many subsequent studies, which have dealt with topics such as temperature in the shear deformation zones [10] and contact surface temperatures between the tool and the chip [11]. Material mechanics approaches (e.g., material testing using a split Hopkinson bar) to describe the combined effects of strain hardening, strain rate, and temperature on flow stress, such as characterized by the Johnson-Cook model, have also been pursued [12]. However, replicating actual processing conditions with a Hopkinson bar is extremely difficult, so this approach has not been widely pursued.

Milling is an important machining process and is widely used in creating automotive parts, aircraft components, etc. As opposed to chip formation in the turning process, the chip thickness in milling changes instantaneously as the angular position of the cutter changes during the process. Early studies focused on the influence of process variables on energy consumption in the orthogonal cutting or turning processes; in those days, limited research was performed on milling processes owing to their complexity.

Building on the 1970s and early 80s research by DeVor and Tlusty, and their respective teams, computer models were developed to predict several performance measures in end milling. The peripheral milling process can be analyzed by discretizing it angle by angle, flute by flute, and finally, after dividing the end mill into axial segments, slice by slice [13]. Figure 1 illustrates the geometry relationship in a peripheral milling process.

One of the most fundamental geometric measures in a cutting process is the chip thickness. In milling, chip thickness can be calculated based on the tool geometry and process kinematics (workpiece geometry plus tool motion path), and then using a simple empirical model, the SCE may be computed. The cutting force system may then be determined based on the chip load and the SCE. The instantaneous chip thickness and average chip thickness calculation may be expressed as [15]:

$$t_c(i,j,k) = f_z \sin\theta(i,j,k) \tag{1}$$

$$\bar{t}_c = \frac{1}{\phi_s}\int_0^{\phi_s} f_z \sin\theta d\theta = \frac{f_z \cdot a_e}{R \cdot \cos^{-1}\left(1-{}^{a_e}/_{R}\right)} \tag{2}$$

$$\theta(i,j,k) = -\theta(j) + (i-1)\frac{2\pi}{Nt} + \left[(k-1)dz + \frac{dz}{2}\right]\cdot\frac{\tan\beta}{R} \tag{3}$$

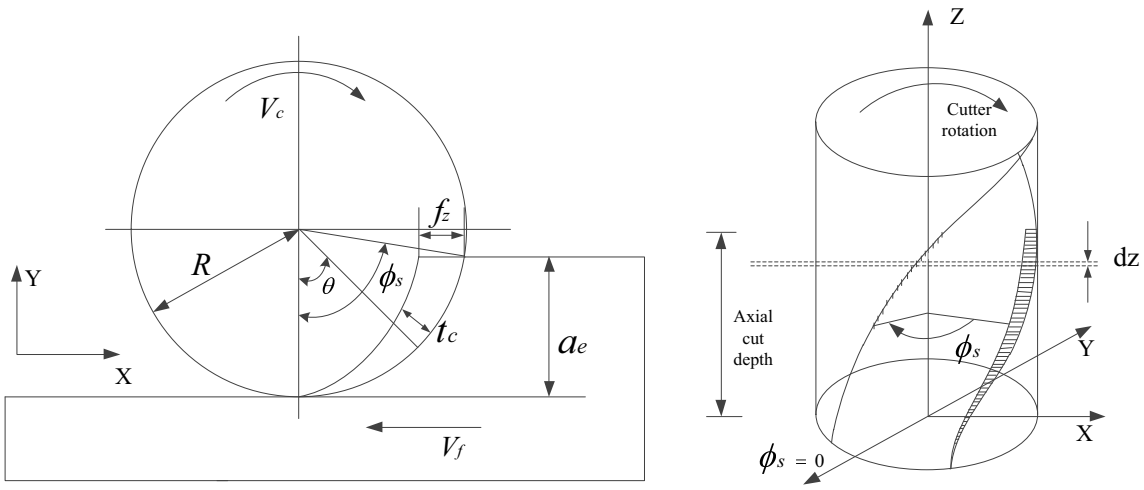

Fig. 1 Peripheral milling geometry relationship schematic diagram [adapted from [13, 14]]

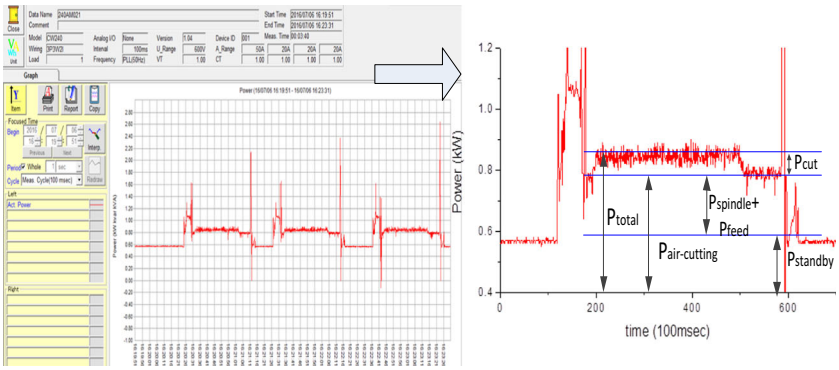

Fig. 2 Milling power profile for a typical test

where f_z is the feed per tooth, $t_c(i,j,k)$ is the instantaneous chip thickness, $\theta(i,j,k)$ is the angular position of the ith axial disk element at the jth angular position of the cutter and the kth flute. $\bar{t}_c$ is the average chip thickness, ϕ_s is the milling engagement angle, a_e is the radial cut depth, R is the tool radius, Nt is the number of tool teeth, β is the helix angle, and dz is the axial height of the disk element. Equations (1)–(3) are applicable to down milling, and similar expressions can be established for up milling [14]. As can be seen from Eqs. (1)–(3), the chip thickness changes during milling and is a function of tool angular position, $\theta(i,j,k)$.

Sabberwal [16] showed that SCE is a function of average chip thickness in milling. Since chip thickness is largely determined by the cutter geometry and cutting parameters, average chip thickness as an intermediate variable captures the effects of cutting conditions on the energy consumption of the milling process. Kline et al. [17] improved the calculation method for chip thickness, considering a cutter runout situation in a follow-up study, and pointed out that while SCE was related to chip thickness, it would be affected by cutter runout. Koenigsberger et al. [18] demonstrated that instantaneous milling force is the product of SCE and chip cross-section area. Their study discussed how the force distribution was affected by the number of tooth engaged during face milling and slab milling. Bayoumi [4] developed instantaneous and mean SCE models through the derivation of milling force, friction force, and friction torque. Additionally, the influence of feed rate on the SCE was discussed under different tool wear and cutting material situations by Bayoumi.

The so-called "size effect" is often suggested as the reason for the presences of the chip thickness in empirical relations for the SCE. Some researchers have considered the size effect and the increased importance of the plowing phenomenon when chip thickness decreases. Fang et al. [19] examined how the size effect changes the SCE. Endres et al. [20] pointed out that the plowing phenomenon would impact SCE and cutting force due to larger friction between the tool flank face and the workpiece surface as the chip thickness tends to zero. Wu et al. [21] asserted that the cutting edge radius and uncut chip thickness have effects on the plowing force which leads changes of SCE.

Studies show that choosing suitable process variables contributes to reduced energy and improved milling performance. Balogun et al. [22] discussed how the ratio of average chip thickness to cutter edge radius (h_M/r_e) affects the relative importance of plowing, and thus energy efficiency and energy waste (since plowing is not as energy efficient as shearing). Shen et al. [23] discovered that same average chip thickness makes the side milling performance similar although radial cutting depth and feed per tooth change. His study also concluded that choosing an appropriate average chip thickness could provide a good machining process performance. Ma et al. [24] researched the effects of tool geometry and cutting parameters on cutting energy in a turning process and provided strategies for minimizing cutting energy.

In summary, many scholars have investigated the effects of process variables on SCE and developed different models to predict SCE and energy consumption. Often, empirical models have been established in the literature; for many of these contributions, mechanistic interpretations are provided to provide insight into the physics that underlie the process. In general, the predictive accuracy of SCE models still needs improvement. Obviously, the SCE model form and the values for the coefficients depend on the cutting conditions examined in experiments that were performed and the assumptions considered. Due to the complexity of the milling process, research focusing on the effects of process variables on SCE during end milling is still lacking, which limits the implementation of

Table 1 Variable (factors) and their levels for Taguchi Orthogonal Array experiment

Factor	Level				
	A	B	C	D	E
n (r/min)	800	1200	1600	2000	2400
V_f(mm/min)	240	290	340	380	420
a_p (mm)	0.5	1	1.5	2	2.5
a_e (mm)	2	3	4	5	6

n, spindle rotation speed; V_f, the table feed rate; a_p, axial cut depth; a_e, radial cut depth

Table 2 Results for L(25) Taguchi Orthogonal Array experiment

No.	n (r/min)	V_f (mm/min)	a_p (mm)	a_e (mm)	MRR (mm^3/s)	V_c (m/s)	f_z (mm/z)	$\bar{t}_c$ (mm)	P_{cut}(kW)	SCE (J/mm^3)
1	800	240	0.5	2	4.00	0.502	0.075	0.0297	0.020	5.00
2	800	290	1	3	14.50	0.502	0.091	0.0433	0.060	4.14
3	800	340	1.5	4	34.00	0.502	0.106	0.0575	0.100	2.94
4	800	380	2	5	63.33	0.502	0.119	0.0705	0.200	3.16
5	800	420	2.5	6	105.00	0.502	0.131	0.0836	0.300	2.86
6	1200	240	1	4	16.00	0.754	0.050	0.0271	0.069	4.31
7	1200	290	1.5	5	36.25	0.754	0.060	0.0359	0.134	3.70
8	1200	340	2	6	68.00	0.754	0.071	0.0451	0.244	3.59
9	1200	380	2.5	2	31.67	0.754	0.079	0.0314	0.119	3.76
10	1200	420	0.5	3	10.50	0.754	0.088	0.0418	0.047	4.48
11	1600	240	1.5	6	36.00	1.005	0.038	0.0239	0.140	3.89
12	1600	290	2	2	19.33	1.005	0.045	0.0180	0.086	4.45
13	1600	340	2.5	3	42.50	1.005	0.053	0.0254	0.155	3.65
14	1600	380	0.5	4	12.67	1.005	0.059	0.0322	0.060	4.74
15	1600	420	1	5	35.00	1.005	0.066	0.0390	0.150	4.29
16	2000	240	2	3	24.00	1.256	0.030	0.0143	0.143	5.96
17	2000	290	2.5	4	48.33	1.256	0.036	0.0196	0.253	5.23
18	2000	340	0.5	5	14.17	1.256	0.043	0.0252	0.068	4.80
19	2000	380	1	6	38.00	1.256	0.048	0.0302	0.178	4.68
20	2000	420	1.5	2	21.00	1.256	0.053	0.0208	0.113	5.38
21	2400	240	2.5	5	50.00	1.507	0.025	0.0148	0.290	5.80
22	2400	290	0.5	6	14.50	1.507	0.030	0.0192	0.115	7.93
23	2400	340	1	2	11.33	1.507	0.035	0.0140	0.085	7.50
24	2400	380	1.5	3	28.50	1.507	0.040	0.0189	0.185	6.49
25	2400	420	2	4	56.00	1.507	0.044	0.0237	0.300	5.36

$\bar{t}_c$, average chip thickness calculated using formula (2); f_z, feed rate per tooth; V_c, cutting speed; the SCE is P_{cut} divided by MRR, tool diameter is 12 mm, and the number of teeth is 4

energy efficiency machining. This work aims to explore how the energy consumption during end milling process is influenced by cutting condition variables and tool geometry. Experimental results are discussed from a cutting mechanism perspective. After that, suggestions are provided to help machining process planners select cutting conditions that provide improved milling energy efficiency.

Table 3 Experimental design to study tool geometry

Tool name	*Nt*	*D* (mm)	Helix angle (°)	Material	Coating
GM-2E-D12.0	2	12	45°	Carbide	TiAlN
GM-4E-D12.0	4	12	45°	Carbide	TiAlN
GM-6E-D12.0	6	12	45°	Carbide	TiAlN
GM-4E-D8.0	4	8	45°	Carbide	TiAlN
GM-4E-D12.0	4	12	45°	Carbide	TiAlN
GM-4E-D16.0	4	16	45°	Carbide	TiAlN

Nt, number of cutting edges; *D*, tool diameter; *TiAlN*, titanium aluminum nitride with 2800 Vickers Hardness and 800 °C oxidation temperature

2 Experiment background and method

A XKA714B/B vertical milling machine was used for all the tests described in this paper. End milling was performed on an AISI 1045 steel workpiece (dimensions: 150 mm × 60 mm × 50 mm). End (or peripheral) milling cutters (provided by Zhuzhou Cemented Carbide Cutting Tools Co. LTD) were used. A Yokogawa CW240 clamp type power meter was used to record power, current, voltage, and other energy-related information during the milling process, and the sampling frequency was set at 100 Hz. The energy consumption analysis software CW Viewer AP240E was used to process and analyze the collected data.

The cutting power during the milling process can be calculated as the difference between the average recorded power during cutting and the average recorded power while "cutting air" as seen in Fig. 2. Each test was repeated three times, and the average cutting power was obtained from these replicates. The milling cutter was inspected frequently and replaced if necessary so that all tests could be performed with a sharp

Table 4 Cutting parameter combination in cutter experiment

Combination	a_e (mm)	a_p (mm)	V_f (mm/min)	n (r/min)	MRR (mm^3/s)
1	2	1	130	1300	4.33
2	4	1	130	1300	8.67
3	6	1	130	1300	13.00

MRR, material removal rate

tool. Coolant was not used for any of the milling process tests. All tests were performed using down milling. Values for the cutting conditions were selected from the recommend parameter ranges provided by the cutting tool manufacturer. More details about the equipment and workpiece material can be found in the Appendix Table 7 and Fig. 13.

The experimental work reported in the paper consisted of two sets of tests:

1) The first set of tests was run using a four fluted end mill with a diameter of 12 mm (Tool GM-4E-D12.0). The cutting parameters (spindle rotation speed, the table feed rate, axial cut depth, and radial cut depth) were varied in this experiment using the levels shown in Table 1 according to an L(25) Taguchi Orthogonal Array. This experimental design consists of 25 combinations of the process variables, from which a suitable empirical relation for SCE may be obtained. The specific test conditions for this experiment and the associated test results are shown in Table 2.

2) The second set of tests (see Table 3) was run by varying the tool geometry. As is evident from the table, changes in the cutter diameter and the number of teeth are considered. It should also be noted that each condition in Table 3 was conducted for the three combinations of cutting parameters shown in Table 4. The purpose of this second set of tests was to characterize the effect of tool geometry on milling energy consumption.

3 Discussion and interpretation of experimental results

3.1 Effect of cutting parameters on milling energy consumption

As was noted previously, two sets of tests are reported in this paper, and the first set of test results is provided in Table 2. In addition to the measured cutting power, the table also lists several additional the calculated values: cutting speed, feed per tooth, average chip thickness, and SCE, the specific cutting energy. Using the results in Table 2, experimental factor range analysis can be obtained and main effect plots for P_{cut}, and SCE are respectively shown in Figs. 3 and 4.

Figure 3 shows that with the increase of a_p, V_f, and a_e, P_{cut} gradually increases, which may due to an increasing MRR. Additionally, with an increase in n, P_{cut} decreases first and then increases. When the n increases, the feed

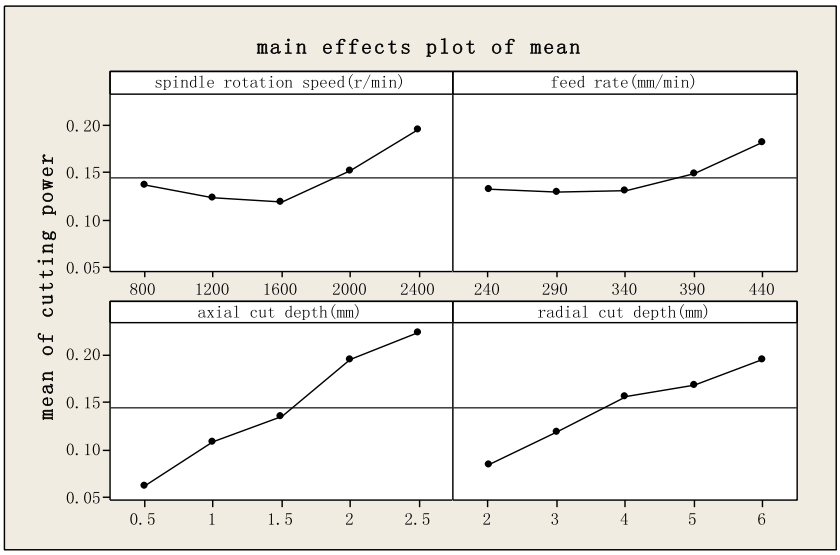

Fig. 3 Factor effect trend for cutting power

Fig. 4 Factor effect trend for SCE

per tooth and the average chip thickness become smaller; in addition, the cutting speed becomes larger; thus, multifactorial effects may cause a nonlinear change of P_{cut}. From Fig. 4, with increases of n, the SCE gradually increase. In addition, with increases of V_f, SCE decreases that may be due to a larger average chip thickness. With increases of a_e, SCE decreases first and then increases that may be because $\bar{t}_c$ is a non-monotonic function of a_e. With increases of a_p, SCE decreases that may be due to increasing chip cross-section. Later, further analysis will be made to explain how these parameters affect SCE in mechanism.

Figure 5 displays the SCE as a function of the MRR. Some past researchers have linked SCE to changes in MRR, and based on the appearance of the graph, there is logic to support this notion: as the MRR increases, the SCE decreases. It is to be noted, however, that while there is a general trend in terms of SCE behavior as a function of MRR, there is substantial variation about the general trend.

Rather than describing SCE as a function of MRR, many past researchers have related SCE to the average chip thickness. Using the results of Table 2, Fig. 6 displays the SCE as a function of average chip thickness. A power function model was fit to this data (again shown in Fig. 4): $SCE = 0.822(\bar{t}_c)^{-0.485}$. As the value for $\bar{t}_c$ grows, the SCE decreases. There appears to be less scatter in this data than in the ($\bar{t}_c$, MRR) data. The behavior depicted in the figure is consistent with what has been reported elsewhere in the literature [18]. The fitted model shown in the figure has a multiple R value of 0.83 (the model describes 83% of the variation in the data). An ANOVA revealed that the model is significant, and an examination of the model residuals revealed no evidence of model inadequacies.

Before proceeding to additional interpretation and discussion of the experimental data, some comments

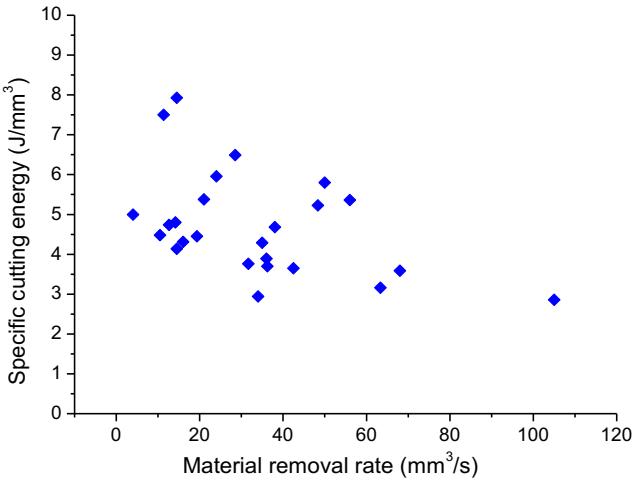

Fig. 5 Effect of MRR on the SCE

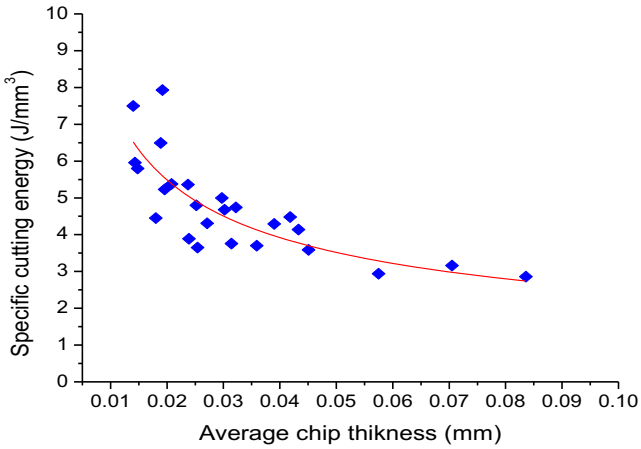

Fig. 6 Specific cutting energy as a function of average chip thickness

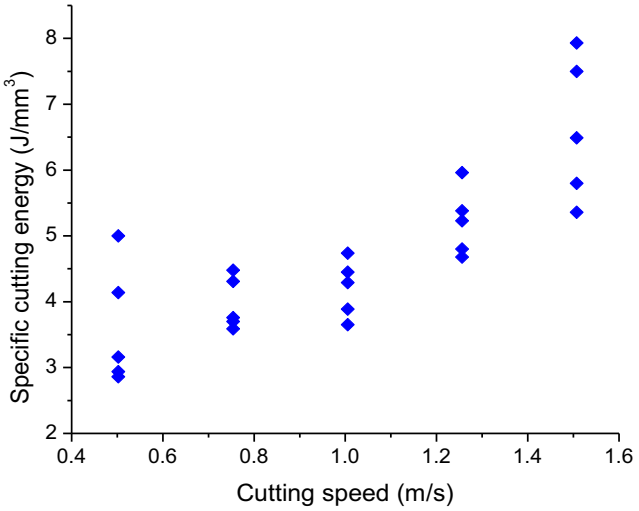

Fig. 7 Effect of cutting speed on SCE

regarding uncertainties in the experimental environment are warranted. Certainly, some errors exist in the experimental measurements and in the estimation of the model coefficients. There are errors in the power measurement due to system noise. For example, the power meter's accuracy is ± 0.6%, and the measuring range accuracy is ± 0.4%. Second, the power test on the machine tool main wire contains some mechanical and electrical additional load loss power during operation, which might affect a little the cutting power calculated. In theory, the additional load loss power is very small [25]. In this study, the cutting power obtained is the sum of additional load loss power and net cutting power.

Figure 7 serves to depict the effect which cutting speed can have on the SCE in end milling. With increases of V_c, many point values of SCE increase. Additionally, point values at each cutting speed are different because of the other experimental factor change.

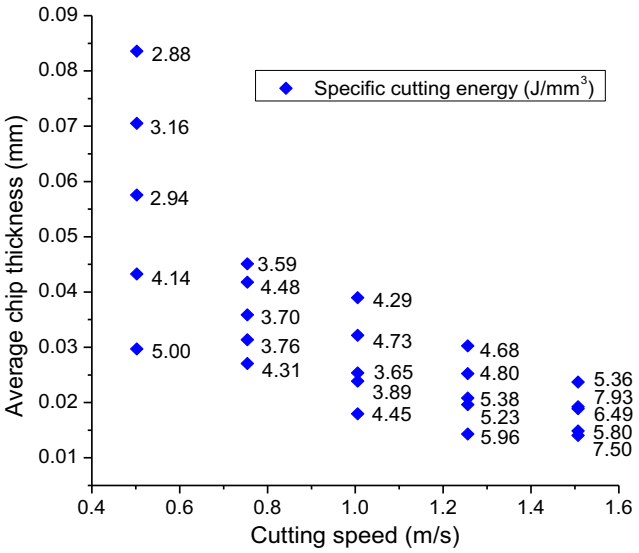

Fig. 8 SCE as a function of cutting speed and average chip thickness

As shown in Fig. 8, it can be considered that SCE is a function of average chip thickness and cutting speed, $SCE = f(\bar{t}_c, V_c)$. As described previously, the shear deformation energy is the main energy that makes the workpiece material produce plastic deformation. When the cutting speed and the average chip thickness change, correspondingly, shear strain, shear strain rate, and temperature in shear deformation zone change and eventually make the cutting energy change.

The shear flow stress τ in the primary shear zone is a function of shear strain γ, shear strain rate $\dot{\gamma}$, and workpiece temperature T_w, deduced by the Johnson-Cook material constitutive model. The SCE is an integral function of shear flow stress. As shown in the following Eqs. (4)–(6), where A (MPa) is the initial yield strength, B (MPa) is strain hardening modulus, n_1 is the strain hardening index, C is the strain rate coefficient, m is the thermal softening index, ε is the normal strain, $\dot{\varepsilon}$ (s^{-1}) is the normal strain rate, $\dot{\varepsilon}_0 = 1.0\,s^{-1}$ is the reference strain rate, T_r (K) is the temperature of the room, and T_{melt} (K) is the melting temperature of the workpiece. More related theory can be found in the literature [26].

$$\sigma = \left[A + B(\varepsilon)^{n_1}\right]\left[1 + C\ln\left(\frac{\dot{\varepsilon}}{\dot{\varepsilon}_0}\right)\right]\left[1-\left(\frac{T_w - T_r}{T_{melt} - T_r}\right)^m\right] \quad (4)$$

$$\sigma = \sqrt{3}\tau \quad \varepsilon = \frac{\gamma}{\sqrt{3}} \quad \dot{\varepsilon} = \frac{\dot{\gamma}}{\sqrt{3}} \quad (5)$$

$$SCE = \int_0^{\gamma} \tau\left(\gamma, \dot{\gamma}, T\right) d\gamma \quad (6)$$

With the decrease of the average cutting thickness, the shear strain increases (shear strain is a function of the effective rake angle and shear angle; when $\bar{t}_c$ is very small, a negative rake angle may occur), the shear strain rate increases (shear strain rate is ratio of shear velocity to shear zone length; when $\bar{t}_c$ decreases, the shear zone length decreases), and the shear zone temperature increases (when $\bar{t}_c$ decreases, more energy is used for shearing and extrusion).

As can be seen in Fig. 8, many point values of the SCE show a tendency to increase when the average cutting thickness decreases because strain and strain rate are more significant for the shear flow stress according to Eqs. (4)–(6).

With the increase of cutting speed, the shear strain rate increases, which may cause the shear flow stress to increase. Moreover, increasing cutting speed makes the

Table 5 Experimental results of different milling tool diameters

D (mm)	N_t	Combination	V_c (m/s)	f_z (mm/tooth)	ϕ_s (°)	$\bar{t}_c$ (mm)	P_{cut} (kW)	SCE (J/mm^3)
8	4	1	0.544	0.025	60.0	0.0247	0.023	5.34
8	4	2	0.544	0.025	90.0	0.0346	0.037	4.22
8	4	3	0.544	0.025	120.0	0.0419	0.049	3.75
12	4	1	0.816	0.025	48.2	0.0203	0.020	4.70
12	4	2	0.816	0.025	70.5	0.0285	0.033	3.84
12	4	3	0.816	0.025	90.0	0.0346	0.042	3.24
16	4	1	1.089	0.025	41.4	0.0176	0.027	6.20
16	4	2	1.089	0.025	60.0	0.0247	0.039	4.47
16	4	3	1.089	0.025	75.5	0.0301	0.051	3.95

thermal diffusion coefficient increase and the temperature higher, which may cause thermal softening and reduce the shear flow stress. These reasons collectively influence the SCE's change. In Fig. 8, many point values of the SCE show the trend of growth with the increase of cutting speed because the shear strain rate has a more significant effect on shear flow stress according to Eqs. (4)~(6). The SCE at some points also shows decreasing trend before $V_c \approx 0.8$ m/s because the thermal softening becomes the main effect on shear flow stress with increasing cutting speed.

3.2 Effect of tool geometry on milling energy consumption

This sub-section discusses the second set of tests results, i.e., how the cutter diameter and the number of teeth influence the SCE during the end milling process.

First, Table 5 shows the results of milling tests with tool diameters, D, of 8 mm, 12 mm, and 16 mm under three combinations of cutting parameters mentioned in Table 4.

It can be found in Table 5 that the feed rate per tooth does not change for different tool diameters at a certain combination. The average chip thickness $\bar{t}_c$ decreases with the increasing tool diameter due to the changes in the milling engagement angle ϕ_s (determined by the ratio of radial cut depth to tool diameter). Figure 9 shows that the SCE decrease with the increase of MRR and $\bar{t}_c$ from combinations 1 to 3 at each tool diameter D. At combination 1, when D increases from 8 to 16 mm, the $\bar{t}_c$ decreases from 0.0247 to 0.0176 mm, and the SCE decreased from 5.34 to 4.70 J/mm^3, and then SCE increased to 6.20 J/mm^3; at combination 2, the $\bar{t}_c$ reduced from 0.0346 to 0.0247 mm, and the SCE decreased from 4.22 to 3.84 J/mm^3, then increased to 4.47 J/mm^3; at combination 3, it can be deduced to the same change trend. In this experiment, when the D increased from 8 to 16 mm, the SCE decreased first and then grew after $V_c = 0.816$ m/s; additionally, the $\bar{t}_c$ decreased by only 29% and the cutting speed V_c increased by 100% on average. A similar trend can be seen in Fig. 7, the SCE decreased first when the cutting speed increased at some points and grew after $V_c \approx 0.8$ m/s. Obviously, V_c becomes a dominant effect

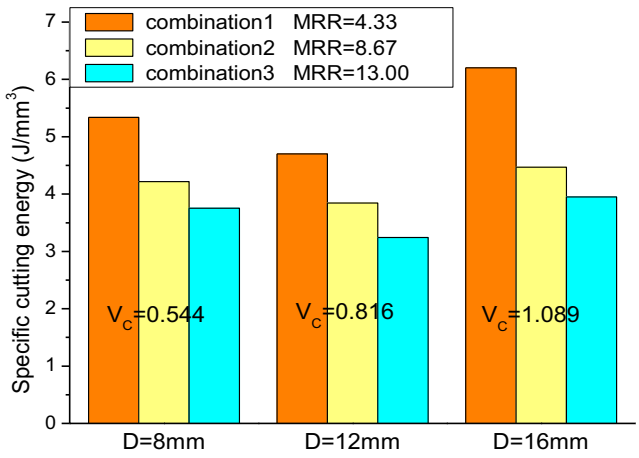

Fig. 9 SCE as a function of tool diameter and the process parameters

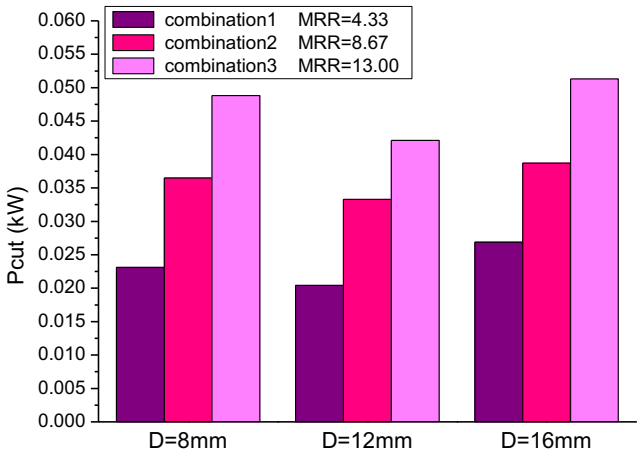

Fig. 10 Cutting power as a function of tool diameter and process parameters

Table 6 Experimental results of different number of teeth

N_t	D (mm)	Combination	V_c (m/s)	f_z (mm/z)	ϕ_s (°)	$\bar{t}_c$ (mm)	P_{cut} (kW)	SCE (J/mm^3)
2	12	1	0.816	0.050	48.2	0.0405	0.015	3.46
2	12	2	0.816	0.050	70.5	0.0569	0.028	3.28
2	12	3	0.816	0.050	90.0	0.0692	0.038	2.91
4	12	1	0.816	0.025	48.2	0.0203	0.020	4.70
4	12	2	0.816	0.025	70.5	0.0285	0.033	3.84
4	12	3	0.816	0.025	90.0	0.0346	0.042	3.24
6	12	1	0.816	0.017	48.2	0.0135	0.022	5.15
6	12	2	0.816	0.017	70.5	0.0190	0.041	4.72
6	12	3	0.816	0.017	90.0	0.0231	0.053	4.06

factor on the SCE when the tool diameter changes. Therefore, when the bigger tool diameter is used, more attention needs to be paid to control the cutting speed in order to reduce the SCE.

From Fig. 10, the relationship between the tool diameter and the average cutting power can be seen. With the increase of tool diameter, cutting power decreases first and then increases. At the same time, the cutting power is also affected by the MRR. At combination 3, the cutting power is larger than any other combination (combination 3 represents a maximum MRR = 13.00 mm^3/s).

Table 6 shows the results of milling tests with teeth number N_t of 2, 4, and 6 under the three combinations of cutting parameter in Table 5.

From Table 6, it can be seen in that the cutting speed and milling engagement angle did not change at the same combination. With the increase of teeth number N_t, the average chip thickness $\bar{t}_c$ decreases due to the changes in feet rate per tooth. Relationships among the teeth number, the process parameters, and the SCE are drawn in Fig. 11. With the increase of teeth number, SCE increase correspondingly. At the combination 1, when the N_t increases from 2 to 6, the SCE increases from 3.46 to 5.15 J/mm^3; at the combination 2, the SCE increased from 3.28 to 4.72 J/mm^3. This analysis similarly can be taken from combination 3. When the N_t increased from 2 to 6, the SCE grew by about 44%, and $\bar{t}_c$ decreased by 67% on average. In this set of experiments, the SCE and the average chip thickness $\bar{t}_c$ change mainly because of changes in feed per tooth f_z with the teeth number changing.

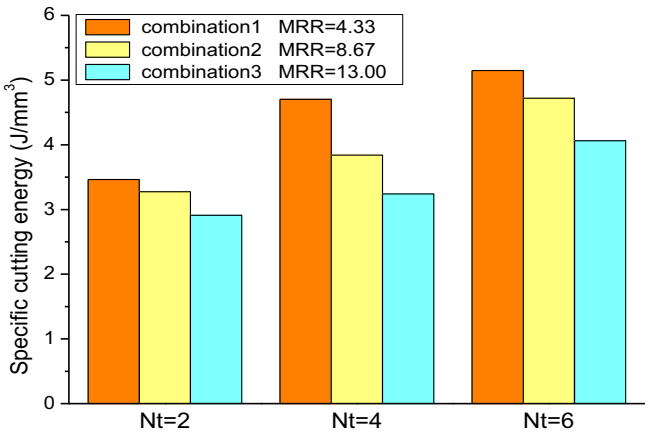

Fig. 11 SCE as a function of number of teeth and process parameters

Figure 12 shows that with an increase in teeth number, cutting power increases. Cutting power is also affected by MRR, and maximum MRR has larger cutting power than any other combination. Although less teeth number makes smaller SCE, it is worth noting that the less teeth number the larger capacity space between teeth may make the average cutting thickness and chip load larger (in $N_t = 2$, $\bar{t}_c$ is bigger than others and cutting power is not very small in Table 6). Thus, appropriate cutting parameters should be chosen to control the cutting force in that situation. In addition, more number of teeth means a dense teeth space that can support a higher material removal rate during the milling process.

4 Conclusion

The study explored how cutting parameters and tool geometry parameters influence energy consumption during end milling through the changed average chip thickness and provides data to support energy consumption assessment of the milling process. Such knowledge helps machining process planners to improve energy efficiency in practical milling processes by relying on quantitative analysis instead of technical experience. Under the experimental scope of this article, the following conclusions are obtained:

The SCE shows the tendency of decrease with increases of average chip thickness. Additionally, the SCE can be decreased or increased as the cutting speed increases. The

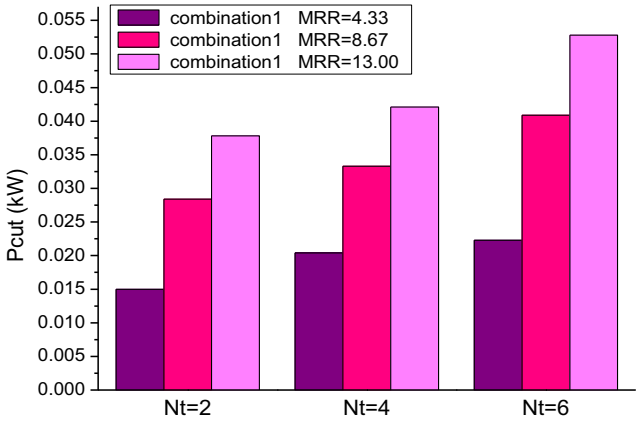

Fig. 12 Cutting power as a function of number of teeth and process parameters

average chip thickness and cutting speed affect the shear strain, shear strain rate, and temperature of the workpiece, which causes changes of the SCE in a mechanism view. If there is an optional range, energy efficient cutting would be obtained by setting a large feed rate per tooth due to decreasing SCE, which needs to consider both n and V_f. Since average chip thickness is a non-monotonic function of radial cut depth, solving for the maximum of chip thickness within the optional range of a_e may make a small SCE.

In this work, when the tool diameter increased from 8 to 16 mm, the V_c increased by 100% and $\bar{t}_c$ decreased by 29% on average. With the cutter diameter increasing, the cutting speed increases which lead to an increased SCE after $V_c \approx 0.8$ m/s, besides the average chip thickness decreases slightly due to the decreasing milling swept angle. Therefore, process planners may select a large material removal rate and suitable cutting speed under a large cutter diameter to reduce SCE gaining energy efficient cutting.

With the number of cutter teeth increasing, feed per tooth decreases; thus, average chip thickness decreases and SCE increases gradually. When the teeth number increased from 2 to 6, the SCE grew by about 44%, and $\bar{t}_c$ decreased by 67% on average. When the teeth number is less, a larger capacity space between teeth makes the average cutting thickness larger. Thus, selecting cutting parameters should be considered to avoid large cutting power that may damage the cutter at less teeth situation. In addition, more teeth number means a dense teeth space that can support a higher material removal rate during the milling process. Thus, an appropriate higher MRR can be set to reduce SCE under the cutting condition of more teeth number.

Acknowledgements Magdalene Jackson is thanked for providing valuable insight and advice.

Funding information Research of this paper is supported by the National Natural Science Foundation of China (NO. 51675314) and Project from Ministry of Industry and Information Technology of China (No. NO.201656261-1-3).

Appendix

Table 7 The experimental equipment details

Name	Information
Cutting tool	Brand: Zhuzhou cemented carbide cutting tools Co., LTD Cutter coating: TiAIN Cutter material: Carbide material Proper material to cut: carbon steel, alloy steel, cast iron.
Cutting material	Grade: 45 Chemical composition mass fraction%: C 0.42~0.50 Si 0.17~0.37 Mn 0.50~0.80 Cr ≤ 0.25 Ni ≤ 0.30 Cu ≤ 0.25 The mechanical properties of | σ_b/MPa = 600 The mechanical properties of | σ_s/MPa = 355 Delivery status without heat treatment, steel hardness of HBS ≤ 229
Machine tool	Brand: XKA714B/B (Beijing No. 1 Machine Tool Plant) Table area (width × length) mm: 400 × 1100 X axis stroke mm: 600 Y axis stroke mm: 450 Z axis stroke mm: 500 Spindle speed mm/min: 500~4000 Feed rate mm/min: (X/Y)6~3200; (Z)3~1600 Fast moving speed mm/min: (X/Y) 8000, (Z) 4000 Positioning accuracy mm: ± 0.015 Spindle motor rated power kW: 5.5/7.5 Spindle torque Nm: 220 Feed torque Nm: 14 Weight kg: 3800 Outline dimension mm: 2130 × 1700 × 2380
Power meter and analysis software	Brand: YOKOGAWA CW240 Power analysis software: CW Viewer AP240E Maximum input voltage: 1000 V Maximum input current: 200 A Frequency range: 45–65 Hz Sample frequency: 100 ms Power reading accuracy: ± 0.6% Power measuring accuracy: ± 0.4% Connection method: three phase wiring
Fitting analysis tool	Origin8

Fig. 13 Experimental installation

Reference

1. International Energy Agency (IEA) (2016) World energy outlook special report 2016 : energy and air pollution. http://www.iea.org/publications/freepublications/publication/WorldEnergyOutlookSpecialReport2016EnergyandAirPollution.pdf. Accessed 23 Aug 2018
2. Gutowski T, Dahmus J, Thiriez A (2006) Electrical energy requirements for manufacturing processes. In: Proceedings of 13th CIRP international conference on life cycle engineering. Leuven, Belgium, pp 5–11
3. Peng T, Xu X (2014) Energy-efficient machining systems: a critical review. Int J Adv Manuf Technol 72(9–12):1389–1406
4. Bayoumi AE, Yücesan G, Hutton DV (1994) On the closed form mechanistic modeling of milling: specific cutting energy, torque, and power. J Mater Eng Perform 3(1):151–158
5. Wang B, Liu ZQ, Song QH, Wan Y, Shi ZY (2016) Proper selection of cutting parameters and cutting tool angle to lower the specific cutting energy during high speed machining of 7050-T7451 aluminum alloy. J Clean Prod 129:292–304
6. Cook NH (1966) Manufacturing analysis, 1st edn. Addison-Wesley Publishing Company, Boston, pp 36–38
7. Merchant ME (1945) Mechanics of the metal cutting process II. Plasticity conditions in orthogonal cutting. J Appl Phys 16:318–324
8. Shaw MC (2004) Metal cutting principles, 2nd edn. Oxford University Press, Oxford
9. Oxley PLB (1962) Shear angle solutions in orthogonal machining. Int J Mach Tool Des Res 2(3):219–229
10. Huang Y, Liang SY (2003) Cutting forces modeling considering the effect of tool thermal property - application to CBN hard turning. Int J Mach Tools Manuf 43(3):307–315
11. Karpat Y, Özel T (2006) Predictive analytical and thermal modeling of orthogonal cutting process-part I: predictions of tool forces, stresses, and temperature distributions. Trans ASME J Manuf Sci Eng 128(2):435–444
12. Lalwani DI, Mehta NK, Jain PK (2009) Extension of Oxley's predictive machining theory for Johnson and Cook flow stress model. J Mater Process Technol 209(12–13):5305–5312
13. Sutherland JW, DeVor RE (1986) An improved method for cutting force and surface error prediction in flexible end milling systems. ASME J Eng Ind 108(4):269–279
14. Kline WA, Devor RE, Lindberg JR (1982) The prediction of cutting forces in end milling with application to cornering cuts. Int J Mach Tool Des Res 22(1):7–22
15. Martellotti ME (1945) An analysis of the milling process: part II-down milling. Trans Am Soc Mech Eng 67:223–251
16. Sabberwal AJP (1962) Cutting forces in down milling. Int J Mach Tool Des Res 2:27–41
17. Kline WA, Devor RE (1983) The effect of runout on cutting geometry and forces in end milling. Int J Mach Tool Des Res 23(2/3):123–140
18. Koenigsberger F, Sabberwal AJP (1961) An investigation into the cutting force pulsations during milling operations. Int J Mach Tool Des Res 1:15–33
19. Fang F, Xu F, Lai M (2015) Size effect in material removal by cutting at nano scale. Int J Adv Manuf Technol 80(1–4):591–598

20. Endres WJ, DeVor RE, Kapoor SG (1995). A dual-mechanism approach to the prediction of machining forces, part 1: Model development. J Manuf Sci E-T ASME 117(4):526–533
21. Wu X, Li L, He N, Hao X, Yao C, Zhong L (2016) Investigation on the ploughing force in microcutting considering the cutting edge radius. Int J Adv Manuf Technol 9(86):2441–2447
22. Balogun VA, Edem IF, Adekunle AA, Mativenga PT (2016) Specific energy based evaluation of machining efficiency. J Clean Prod 116:187–197
23. Shen Z, Sun X, Liu G, Chen M (2007) The milling mechanism of Ti6Al4V based on average cutting thickness. J Shanghai Jiaotong U 41(4):614–618 (in Chinese)
24. Ma J, Ge X, Chang S, Lei S (2014) Assessment of cutting energy consumption and energy efficiency in machining of 4140 steel. Int J Adv Manuf Technol 74(9–12):1701–1708
25. Lv JX, Tang RZ, Jia S (2014) Therblig-base d energy supply modeling of computer numerical control machine tools. J Clean Prod 65:168–177
26. Johnson GR, Cook WH (1983) A constitutive model and data for metals subjected to large strains, high strain rates and high temperatures. In Proceedings of the 7th International Symposium on Ballistics 21(1):541–547